JACS
JOURNAL OF THE AMERICAN CHEMICAL SOCIETY
pubs.acs.org/JACS
Article

CO_2 Hydrogenation to Formate and Formic Acid by Bimetallic Palladium–Copper Hydride Clusters

Gaoxiang Liu,[#] Patricia Poths,[#] Xinxing Zhang,* Zhaoguo Zhu, Mary Marshall, Moritz Blankenhorn, Anastassia N. Alexandrova,* and Kit H. Bowen*

Cite This: J. Am. Chem. Soc. 2020, 142, 7930–7936
Read Online

ACCESS | Metrics & More | Article Recommendations | Supporting Information

ABSTRACT: Mass spectrometric analysis of the anionic products of interaction between bimetallic palladium–copper tetrahydride anions, $PdCuH_4^-$, and carbon dioxide, CO_2, in a reaction cell shows an efficient generation of the $PdCuCO_2H_4^-$ intermediate and formate/formic acid complexes. Multiple structures of $PdCuH_4^-$ and $PdCuCO_2H_4^-$ are identified by a synergy between anion photoelectron spectroscopy and quantum chemical calculations. The higher energy $PdCuH_4^-$ isomer is shown to drive the catalytic hydrogenation of CO_2, emphasizing the importance of accounting for higher energy isomers for cluster catalytic activity. This study represents the first example of CO_2 hydrogenation by bimetallic hydride clusters.

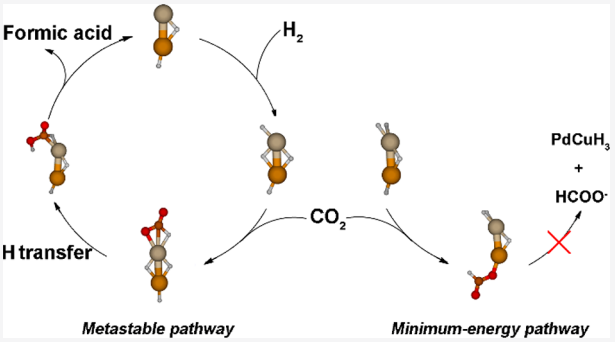

INTRODUCTION

Transforming CO_2 into reduced, value-added molecules is of great interest for environmental and economic reasons. For catalytic CO_2 functionalization, bimetallic catalysts have shown improved activity and selectivity over single-component ones, as lattice engineering can be utilized to tailor the surface and electronic structures of bimetallic catalysts and thus to regulate their performance.[1−4] The rational design of high-efficiency bimetallic catalysts demands a mechanistic understanding of how the catalytic CO_2 transformation processes on the active sites. Although it is well-established that the formation of metal hydrides and the insertion of CO_2 into the metal–hydrogen bond are the critical steps in CO_2 hydrogenation, comprehensive knowledge about them remains limited because of a lack of direct experimental characterization on these key reaction intermediates.[5−9] In particular, it is less clear how the interplay between different metals can alter catalyst properties, including hydrogen and CO_2 binding sites, electronic structures, charge-transfer property, and release of products, all of which influence catalytic performance.

Synergy between the experimental characterization of reaction intermediates and state-of-the-art quantum chemistry calculations enables gas-phase studies of CO_2 reduction and hydrogenation to provide mechanistic insight into CO_2 functionalization at the molecular level.[10−18] Although single-metal hydrides (e.g., Cp_2TiH^+,[14] PtH_3^-,[15] FeH^-,[16] and $Cu_{1,2}H_2^-$[17,18]) can convert CO_2 into formate and formate complexes, we are not aware of the use of bimetallic hydrides for CO_2 hydrogenation. The present work focuses on the hydrogenation of CO_2 via reaction with the anionic bimetallic palladium–copper tetrahydride cluster, $PdCuH_4^-$. We selected the palladium–copper hydride because its reaction with CO_2 is an ideal model for understanding the hydrogenation process over bimetallic palladium–copper catalysts, which have shown superior CO_2 hydrogenation activity compared to single-component palladium or copper catalysts.[19−23] We show that a metastable $PdCuH_4^-$ isomer catalytically converts CO_2 to formic acid, in-line with recent theoretical predictions reporting catalysis on fluxional clusters can be driven by less stable but more active cluster isomers accessible in reaction conditions.[24−30]

RESULTS AND DISCUSSION

$PdCuH_4^-$ was prepared in a pulsed arc cluster ionization source (PACIS), which has been applied to the generation of various metal hydrides.[31,32] Briefly, an ∼30 μs duration, ultrahigh voltage, and current discharge were used to vaporize Pd and Cu powders. Almost simultaneously, high-pressure hydrogen gas was injected into the discharge region. The resulting mixture of atoms, ions, and electrons reacted to form $PdCuH_4^-$. $PdCuH_4^-$ clusters were then collisionally cooled and carried downstream by the supersonically expanding hydrogen gas to interact with CO_2 in a reaction cell,[15,33,34] where additional energy as high as 1 eV can be provided to the

Received: February 16, 2020
Published: April 6, 2020

https://dx.doi.org/10.1021/jacs.0c01855
J. Am. Chem. Soc. 2020, 142, 7930–7936

reaction via the multicollisions with the fastest H_2 molecules in the Maxwell–Boltzmann distribution. The resultant anionic products were identified by time-of-flight mass spectrometry. Figure 1 presents mass spectra with or without CO_2. With no

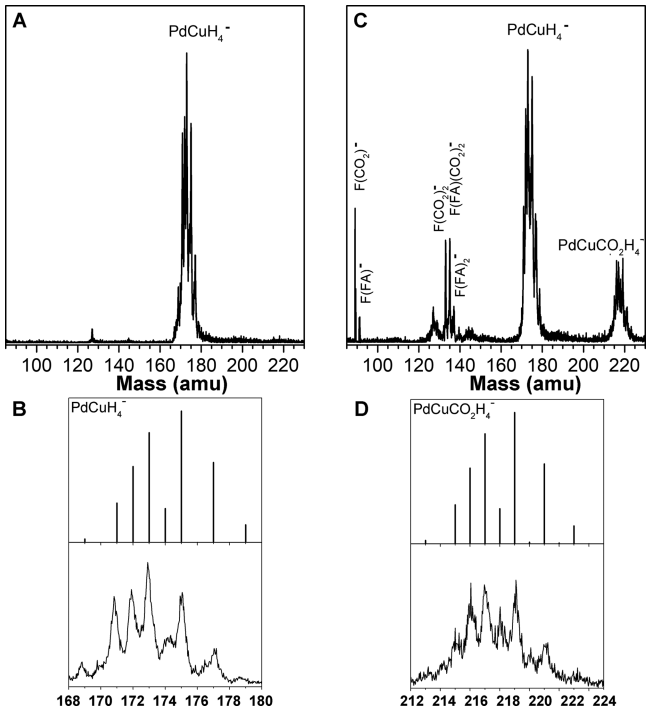

Figure 1. (A) Mass spectrum of $PdCuH_4^-$ cluster anions. (B) Simulated and experimental mass spectra of $PdCuH_4^-$. (C) Mass spectrum of $PdCuH_4^-$ reacting with CO_2. (D) Simulated and experimental mass spectra of $PdCuCO_2H_4^-$. "F" indicates formate. "FA" indicates formic acid.

CO_2 in the reaction cell, we observed the mass series of $PdCuH_4^-$ (Figure 1A), and its match with the simulated isotopic pattern confirms $PdCuH_4^-$ as the only palladium–copper hydride formed under our experimental conditions (Figure 1B). When CO_2 was added to the reaction cell, prominent mass series appeared at masses both higher and lower than $PdCuH_4^-$ (Figure 1C). The higher-mass series is the reaction intermediate $PdCuCO_2H_4^-$, which was identified by comparing the experimental and simulated isotopic patterns (Figure 1D). The lower-mass peaks are formate- and formic acid containing anionic clusters. The tagging of formic acid to anionic formate made possible the observation of this neutral molecule by mass spectrometry. The high summed intensity of formate and formic acid products indicates that $PdCuH_4^-$ hydrogenates CO_2 efficiently. Note that the observation of formic acid suggests the reaction

$$PdCuH_4^- + CO_2 \rightarrow PdCuH_2^- + HCOOH \text{ (formic acid)}$$

yet $PdCuH_2^-$ or other palladium–copper hydrides were absent after $PdCuH_4^-$ reacted with CO_2. This implies regeneration of $PdCuH_4^-$ via H_2 absorption to $PdCuH_2^-$. Therefore, we proposed that the catalytic reaction

$$H_2 + CO_2 \xrightarrow{PdCuH_4^-} HCOOH$$

had occurred under our experimental conditions.

We then applied anion photoelectron spectroscopy to characterize $PdCuH_4^-$ and $PdCuCO_2H_4^-$ (Figure 2). For

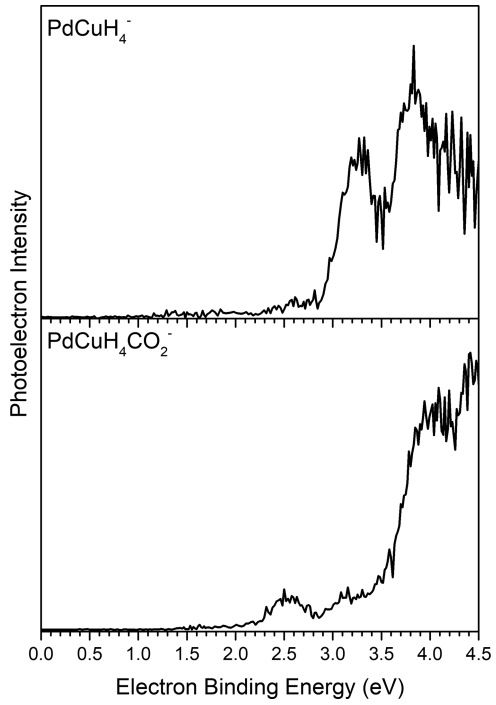

Figure 2. Photoelectron spectra of $PdCuH_4^-$ (A) and $PdCuCO_2H_4^-$ (B) measured with 266 nm (4.66 eV) photons.

$PdCuH_4^-$, two electron binding energy (EBE) peaks at 3.36 and 3.83 eV are assigned as the vertical detachment energies (VDE). The VDE is defined as the photodetachment transition energy at which the Franck–Condon overlap is at its maximum between the anion's vibrational wave function and that of its neutral counterpart with both in their ground electronic states. For $PdCuCO_2H_4^-$, its VDE values are 2.49, 3.93, and 4.40 eV.

Figure 3 shows the calculated structures that are confirmed to account for the experimentally measured PES. Structures **A** and **B** are two low-energy $PdCuH_4^-$ isomers, the latter 0.46 eV higher in energy. These two structures differ only in the location of one H atom—both have the same low-spin state (multiplicity 1). On the basis of the similar charges on the metal centers across both structures, it does not appear that there is a significant change in the formal oxidation state of each metal between A and B. Structures **C**, **D**, and **E** are isomers of $PdCuCO_2H_4^-$ derived from CO_2 reacting with **A** and **B**. In structure **C**, CO_2 is inserted into the Cu–H bond of structure **A**. Structure **D**, on the other hand, is obtained by CO_2 association with the Pd and H atoms in structure **B**. Both structures **C** and **D** have a formate moiety, the latter being 0.92 eV higher in energy. For structure **D**, the H atom that bridges Pd and Cu atoms can further transfer to the formate moiety, forming structure **E** with a formic acid moiety. The dissociation of structure **E** into formic acid and $PdCuH_2^-$, which is structure **F**, may explain the observation of formic acid in the experiment. All structures are in their respective low-spin states. On the basis of the atomic charges of all of the structures, it appears that both Pd and Cu are in their 0 oxidation state throughout. The H ligands instead experience the most significant changes in the charge.

The verification of these calculated structures was accomplished by calculating their VDEs at the CCSD//UPBEPBE/aug-cc-pvtz+pp level of theory and comparing

https://dx.doi.org/10.1021/jacs.0c01855
J. Am. Chem. Soc. 2020, 142, 7930–7936

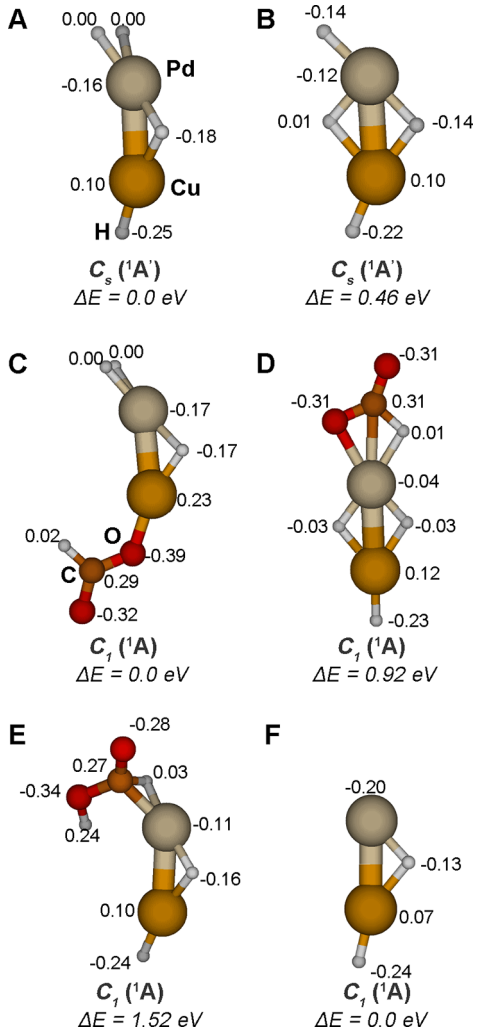

Figure 3. Calculated relevant lowest energy structures of $PdCuH_4^-$ (A and B), $PdCuCO_2H_4^-$ (C, D, and E), and $PdCuH_2^-$ (F). Symmetry, spectroscopic label, and energy relative to the global minimum structure of the same stoichiometry are shown below each structure. The charge on each atom is also shown.

Table 1. Computed VDEs for Each Structure from Figure 3 and Their Corresponding Experimental Values[a]

	$PdCuH_4^-$		$PdCuCO_2H_4^-$			$PdCuH_2^-$
structure:	A	B	C	D	E	F
expt. VDE	3.83	3.36	4.40	N/A[b]	3.93	2.49
calc. VDE	3.71	3.51	4.36	5.44	3.79	2.25

[a]All VDE values are given in eV. [b]This structure's EBE is higher than the photon energy of the photodetachment laser.

them with the experimental values (Table 1). For $PdCuH_4^-$, structures **A** and **B** respectively match the higher and the lower EBE feature in the experimental photoelectron spectrum. For the $PdCuCO_2H_4^-$ spectrum, the feature at 4.40 eV is attributable to structure **C**, and the feature at 3.93 eV is due to photodetachment of structure **E**. The feature at 2.49 eV does not match the calculated VDE of any $PdCuCO_2H_4^-$ structure. Instead, it agrees with the calculated VDE of structure **F**. This suggests that during photodetachment, $PdCuCO_2H_4^-$ was also photodissociated into $PdCuH_2^-$ (structure **F**) and formic acid. The dissociation product $PdCuH_2^-$ was subsequently photodetached, contributing the 2.49 eV feature in the $PdCuCO_2H_4^-$ spectrum. To support this statement, we took the $PdCuH_4CO_2^-$ spectra with different laser power while keeping other collection conditions unchanged. The photoelectron intensity of the feature at 2.49 eV, I, shows a nonlinear dependence on the laser power, P, which can be represented by $I \propto P^{1.67}$ (Figure S1, Supporting Information). This suggests that it is the two-photon process that primarily contributes to this feature. This photodissociation/photodetachment phenomenon has been observed in our previous photodetachment experiment on anionic metal-hydride-CO_2 adducts.[15] Structure **D** should be present despite having a calculated VDE beyond the range of the photodetachment laser, as structure **E** is derived from it. Therefore, the two $PdCuH_4^-$ and three $PdCuCO_2H_4^-$ isomers were all observed experimentally. The high-energy environment in PACIS enables the formation of $PdCuH_4^-$ clusters with different energies,[35] which were subsequently cooled to their ground electronic states before interacting with CO_2.

The observation of two isomers of $PdCuH_4^-$ and their respective CO_2 insertion complexes suggests two reaction mechanisms beginning from structures **A** and **B**. Figure 4 presents the two calculated reaction pathways. The pathway in red is initiated by structure **A**, whereas the pathway in blue starts with structure **B**. When structure **A** interacts with CO_2, CO_2 inserts into its Cu−H bond without a barrier, forming structure **C**. This insertion step is exothermic by 1.32 eV. Structure **C**, however, is a very stable adduct, as seen by the high energy required for it to release formate as the product. The high dissociation energy of 2.38 eV according to calculations is unlikely to occur under the multicollision conditions in the reaction cell. Therefore, it is unlikely that the formate observed in the experiment formed via this mechanism. The reaction starting from structure **B**, on the other hand, proceeds on a smoother potential energy surface. Upon interaction, CO_2 is associated with the Pd and H atoms to form structure **D**. The transition from structure **B** to **D** is also barrierless. An H atom that bridges the Pd and Cu atoms in structure **D** subsequently transfers to the formate moiety, forming structure **E**, with an activation barrier 0.95 eV above that of structure **D** or 0.09 eV above that of the entrance channel. The dissociation of structure **E** into $PdCuH_2^-$ and formic acid is endothermic by 0.80 eV. Therefore, all steps on the structure **B** initiated pathway are within 0.5 eV of the entrance channel energy, making them accessible under the experimental conditions where excess energy is provided via multicollisions with the fast-moving H_2 molecules.[36,37] When electrons are present in the reaction environment, the released formic acid can deprotonate to yield formate via the dissociate electron attachment, a common acid−electron interaction in the gas phase. As mentioned earlier, the reaction does not stop at the $PdCuH_2^-$ ion; there is no evidence of it in the mass spectrum, suggesting that in the presence of abundant H_2 in the reaction cell, the following reaction takes place:

$$H_2 + PdCuH_2^- \rightarrow PdCuH_4^-$$

This reaction is 0.87 eV exothermic if forming structure **A** or 0.41 eV exothermic if leading to structure **B**. Thus, the H_2 environment readily regenerates the $PdCuH_4^-$ clusters, completing the catalytic cycle.

Compared to Cu, Pd is stronger in binding H but weaker in binding O.[5] Therefore, the structure with more H binding to Pd is more stable. Because structure **A** has one H atom that

https://dx.doi.org/10.1021/jacs.0c01855
J. Am. Chem. Soc. 2020, 142, 7930−7936

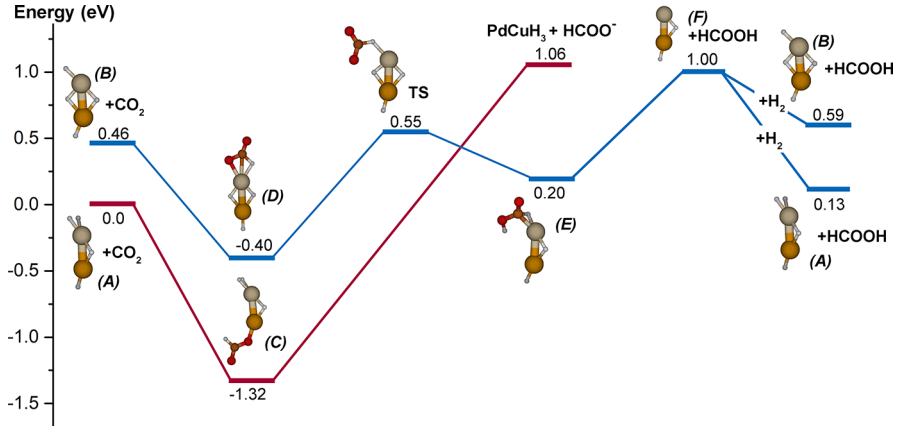

Figure 4. Profile for the reaction of CO_2 with $PdCuH_4^-$. Zero-point energy corrected energies are given in eV. The letters in the parentheses correspond to their labels in Figure 3. The potential energy surface is referenced to the total energy of structure **A** and an isolated CO_2.

binds exclusively to Pd rather than both Pd and Cu, it is lower in energy than structure **B**. For structure **A**, however, the binding of more H exclusively to Pd inhibits the binding of CO_2 on Pd.[38] Instead, CO_2 inserts into the Cu−H bond, forming the strong Cu−O bond (structure **C**). The high dissociation energy of the Cu−O bond prevents the release of formate product, ending this pathway in a "catalytic deadlock". In structure **B**, Pd is more exposed while Cu is more coordinated, which facilitates the initial CO_2 binding to the Pd atom. Because Pd has weak O binding, the formic acid moiety associates with Pd via Pd−C and Pd−H interactions, as shown in structure **E**. Dissociation of the formic acid product is thus much less endothermic with this reaction pathway. Also, importantly, the Pd site becomes exposed after release of the formic acid and can readily absorb an H_2 molecule to complete the catalytic cycle. This result echoes recent reports emphasizing the metastable structures as the actual active sites in cluster catalysis.[28]

The charge analysis can further rationalize the different reactivity of the two $PdCuH_4^-$ clusters (Figure 3). The calculated atomic charges show a difference in the charge distributions in CO_2 bound to structures **A** and **B**. When CO_2 is bound to Cu, as in structure **C**, the charge difference between Cu and the formate fragment is more significant than the analogous charge difference between Pd and the formate fragment. Furthermore, Cu is positively charged, whereas Pd is negatively charged, so the formate moiety interacts more strongly with Cu.

CONCLUSIONS

To summarize, we have demonstrated that the bimetallic $PdCuH_4^-$ clusters can convert CO_2 into formate and formic acid. Mass spectrometric analysis of the reaction products between $PdCuH_4^-$ and CO_2 reveals the reaction intermediate $PdCuCO_2H_4^-$, the reaction products formate and formic acid, and the regeneration of $PdCuH_4^-$, completing the catalytic cycle. Different isomers of $PdCuH_4^-$ and $PdCuCO_2H_4^-$ are identified by anion photoelectron spectroscopy and electronic structure calculations. Mechanistic study confirms metastable structures as the catalytic driving force. This work represents the first example of CO_2 hydrogenation by bimetallic hydride clusters, providing insight into understanding the catalytic properties of bimetallic catalysts.

METHODS

Experimental Methods. The experimental technique, anion photoelectron spectroscopy, is conducted by crossing a mass-selected beam of negative ions with a fixed-energy photon beam and energy analyzing the resulting photodetached electrons. This technique is governed by the energy-conservation relationship, $h\nu$ = EBE + EKE, where $h\nu$, EBE, and EKE are the photon energy, electron binding (transition) energy, and the electron kinetic energy, respectively. Our photoelectron spectrometer, which has been described previously,[39] consists of one of several ion sources, a linear time-of-flight (TOF) mass spectrometer, a mass gate, a momentum decelerator, a neodymium-doped yttrium aluminum garnet (Nd:YAG) laser for photodetachment, and a magnetic bottle electron energy analyzer. Photoelectron spectra were calibrated against the well-known photoelectron spectrum of Cu^-. The $PdCuH_4^-$ anions were generated using a pulsed-arc (discharge) cluster ionization source (PACIS), which has been described in detail elsewhere.[40] This cluster anion source has been used to generate a variety of transition-metal hydride cluster anions.[32,41−43] It provided us with a broad range of cluster sizes and compositions. During PACIS operation, a 30 μs long, ~4000 V electrical pulse applied across the anode and the mixed Pd/Cu pressed-powder cathode in the discharge chamber vaporizes the Pd and Cu atoms. Almost simultaneously with the discharge, 180 psi of ultra-high-purity hydrogen gas was injected into the discharge region, where it was dissociated into hydrogen atoms. The resulting mixture of atoms, ions, and electrons then reacted and cooled as it expanded through the PACIS housing. After a small gap, this flow then continued through a 15 cm long collision/reactor cell before exiting into a high vacuum. For initiation of the reaction between CO_2 and $PdCuH_4^-$, pure CO_2 was injected into the collision cell using a second pulsed valve. The resultant anions then drifted through a skimmer, through a differentially pumped region, and into the TOF region, where they were perpendicularly extracted and mass-selected prior to photodetachment. Because of palladium's and copper's isotope patterns and the presence of multiple hydrogen atoms, photoelectron spectra were taken at all observed mass peaks.

Computational Methods. The calculated structures presented in this work were computed using density functional theory (DFT), using the PBEPBE[44] functional in Gaussian16.[45] The initial structure search was performed using the LANL2DZ[46−48] basis set, after which the lowest energy structures were further optimized using the aug-cc-pvtz+pp[49] basis set. After geometry optimization, the energies of the anionic and neutral clusters were calculated at the CCSD[50−53]//UPBE level to determine the vertical detachment energies (VDE) for each structure for comparison with experimental PES results. CASSCF (m,n)[54−62] up to (14,14) was run to verify the accuracy of the single reference method. CCSD//UPBE was used rather than TD-DFT for VDE calculations because of the unreliability of the result as the functional was changed, and CCSD(T) was not used as

https://dx.doi.org/10.1021/jacs.0c01855
J. Am. Chem. Soc. 2020, 142, 7930−7936

perturbation theory failed for some structures. Only the first VDE was calculated for each structure—if there are VDE2+ peaks present in the spectrum, they are not accounted for, but all peaks present in the experimental spectrum have corresponding computed VDEs. Charges on each atom were calculated using natural population analysis.[63]

■ ASSOCIATED CONTENT

Supporting Information

The Supporting Information is available free of charge at https://pubs.acs.org/doi/10.1021/jacs.0c01855.

Figure showing the photoelectron spectra of $PdCuH_4CO_2^-$ as well as the relationship between the integrated photoelectron intensity and the laser power; coordinates of all structures (PDF)

■ AUTHOR INFORMATION

Corresponding Authors

Kit H. Bowen − *Department of Chemistry, Johns Hopkins University, Baltimore, Maryland 21218, United States;* orcid.org/0000-0002-2858-6352; Email: kbowen@jhu.edu

Anastassia N. Alexandrova − *Department of Chemistry and Biochemistry, University of California, Los Angeles, Los Angeles, California 90095-1569, United States;* orcid.org/0000-0002-3003-1911; Email: ana@chem.ucla.edu

Xinxing Zhang − *Key Laboratory of Advanced Energy Materials Chemistry (Ministry of Education), Renewable Energy Conversion and Storage Center (ReCAST), College of Chemistry, Nankai University, Tianjin 300071, China;* orcid.org/0000-0001-5884-2727; Email: zhangxx@nankai.edu.cn

Authors

Gaoxiang Liu − *Department of Chemistry, Johns Hopkins University, Baltimore, Maryland 21218, United States;* orcid.org/0000-0002-1001-0064

Patricia Poths − *Department of Chemistry and Biochemistry, University of California, Los Angeles, Los Angeles, California 90095-1569, United States*

Zhaoguo Zhu − *Department of Chemistry, Johns Hopkins University, Baltimore, Maryland 21218, United States*

Mary Marshall − *Department of Chemistry, Johns Hopkins University, Baltimore, Maryland 21218, United States*

Moritz Blankenhorn − *Department of Chemistry, Johns Hopkins University, Baltimore, Maryland 21218, United States*

Complete contact information is available at: https://pubs.acs.org/10.1021/jacs.0c01855

Author Contributions

[#]G. L. and P. P. contributed equally to this manuscript.

Notes

The authors declare no competing financial interest.

■ ACKNOWLEDGMENTS

This material is based upon work supported by the Air Force Office of Scientific Research (AFOSR) under Grant No. FA9550-19-1-0077 (K.H.B.) and DOE-BES Grant No. DE-SC0019152 to A.N.A. CPU resources at the National Energy Research Scientific Computing Center (NERSC), and XSEDE were used. X. Z. acknowledges the National Key R&D Program of China (2018YFE0115000) and the NSF of Tianjin City (19JCYBJC19600).

■ REFERENCES

(1) Gilroy, K. D.; Ruditskiy, A.; Peng, H.-C.; Qin, D.; Xia, Y. Bimetallic nanocrystals: syntheses, properties, and applications. *Chem. Rev.* **2016**, *116* (18), 10414.

(2) Kim, D.; Xie, C.; Becknell, N.; Yu, Y.; Karamad, M.; Chan, K.; Crumlin, E. J.; Nørskov, J. K.; Yang, P. Electrochemical activation of CO_2 through atomic ordering transformations of AuCu nanoparticles. *J. Am. Chem. Soc.* **2017**, *139*, 8329−8336.

(3) Mori, K.; Sano, T.; Kobayashi, H.; Yamashita, H. Surface engineering of a supported PdAg catalyst for hydrogenation of CO_2 to formic acid: elucidating the active Pd atoms in alloy nanoparticles. *J. Am. Chem. Soc.* **2018**, *140*, 8902−8909.

(4) Vasileff, A.; Xu, C.; Jiao, Y.; Zheng, Y.; Qiao, S.-Z. Surface and interface engineering in copper-based bimetallic materials for selective CO_2 electroreduction. *Chem.* **2018**, *4*, 1809−1831.

(5) Tang, Q.; Lee, Y.; Li, D.-Y.; Choi, W.; Liu, C. W.; Lee, D.; Jiang, D. Lattice-hydride mechanism in electrocatalytic CO_2 reduction by structurally precise copper-hydride nanoclusters. *J. Am. Chem. Soc.* **2017**, *139*, 9728−9736.

(6) Zhu, S.; Jiang, B.; Cai, W.; Shao, M. Direct observation on reaction intermediates and the role of bicarbonate anions in CO_2 electrochemical reduction reaction on Cu surfaces. *J. Am. Chem. Soc.* **2017**, *139*, 15664−15667.

(7) Mori, K.; Sano, T.; Kobayashi, H.; Yamashita, H. Surface engineering of a supported PdAg catalyst for hydrogenation of CO_2 to formic acid: elucidating the active Pd atoms in alloy nanoparticles. *J. Am. Chem. Soc.* **2018**, *140*, 8902−8909.

(8) Kato, S.; Matam, S. K.; Kerger, P.; Bernard, L.; Battaglia, C.; Vogel, D.; Rohwerder, M.; Zuttel, A. The origin of the catalytic activity of a metal hydride in CO_2 reduction. *Angew. Chem., Int. Ed.* **2016**, *55*, 6028−6032.

(9) Wang, W.-H.; Himeda, Y.; Muckerman, J. T.; Manbeck, G. F.; Fujita, E. CO_2 hydrogenation to formate and methanol as an alternative to photo-and electrochemical CO_2 reduction. *Chem. Rev.* **2015**, *115*, 12936−12973.

(10) Green, A. E.; Justen, J.; Schöllkopf, W.; Gentleman, A. S.; Fielicke, A.; Mackenzie, S. R. IR Signature of Size-Selective CO_2 Activation on Small Platinum Cluster Anions, Pt_n−(n= 4−7). *Angew. Chem., Int. Ed.* **2018**, *57*, 14822−14826.

(11) Liu, G.; Ciborowski, S. M.; Zhu, Z.; Chen, Y.; Zhang, X.; Bowen, K. H. The metallo-formate anions, M (CO_2)−, M= Ni, Pd, Pt, formed by electron-induced CO_2 activation. *Phys. Chem. Chem. Phys.* **2019**, *21*, 10955−10960.

(12) Dodson, L. G.; Thompson, M. C.; Weber, J. M. Characterization of intermediate oxidation states in CO_2 activation. *Annu. Rev. Phys. Chem.* **2018**, *69*, 231−252.

(13) Thompson, M. C.; Ramsay, J.; Weber, J. M. Solvent-driven reductive activation of CO_2 by bismuth: switching from metalloformate complexes to oxalate products. *Angew. Chem., Int. Ed.* **2016**, *55*, 15171−15174.

(14) Tang, S.; Rijs, N. J.; Li, J.; Schlangen, M.; Schwarz, H. Ligand-Controlled CO_2 Activation Mediated by Cationic Titanium Hydride Complexes,[LTiH]+(L= Cp2, O). *Chem. - Eur. J.* **2015**, *21*, 8483−8490.

(15) Zhang, X.; Liu, G.; Meiwes-Broer, K.; Gantefor, G.; Bowen, K. CO_2 activation and hydrogenation by PtHn− cluster anions. *Angew. Chem., Int. Ed.* **2016**, *55*, 9644−9647.

(16) Jiang, L.; Zhao, C.; Li, X.; Chen, H.; He, S.-G. Formation of Gas-Phase Formate in Thermal Reactions of Carbon Dioxide with Diatomic Iron Hydride Anions. *Angew. Chem., Int. Ed.* **2017**, *56*, 4187−4191.

(17) Liu, Y.-Z.; Jiang, L.-X.; Li, X.-N.; Wang, L.-N.; Chen, J.-J.; He, S.-G. Gas-phase reactions of carbon dioxide with copper hydride anions Cu_2H_2−: Temperature-dependent transformation. *J. Phys. Chem. C* **2018**, *122*, 19379−19384.

(18) Pascher, T. F.; Oncak, M.; van der Linde, C.; Beyer, M. K. Release of Formic Acid from Copper Formate: Hydride, Proton-Coupled Electron and Hydrogen Atom Transfer All Play their Role. *ChemPhysChem* **2019**, *20*, 1420−1424.

(19) Ma, S.; Sadakiyo, M.; Heima, M.; Luo, R.; Haasch, R. T.; Gold, J. I.; Yamauchi, M.; Kenis, P. J. A. Electroreduction of carbon dioxide to hydrocarbons using bimetallic Cu−Pd catalysts with different mixing patterns. *J. Am. Chem. Soc.* **2017**, *139*, 47−50.
(20) Gao, D.; Zhou, H.; Cai, F.; Wang, J.; Wang, G.; Bao, X. Pd-containing nanostructures for electrochemical CO_2 reduction reaction. *ACS Catal.* **2018**, *8*, 1510−1519.
(21) Kyriakou, G.; Boucher, M. B.; Jewell, A. D.; Lewis, E. A.; Lawton, T. J.; Baber, A. E.; Tierney, H. L.; Flytzani-Stephanopoulos, M.; Sykes, E. C. H. Isolated metal atom geometries as a strategy for selective heterogeneous hydrogenations. *Science* **2012**, *335*, 1209−1212.
(22) Long, R.; Li, Y.; Liu, Y.; Chen, S.; Zheng, X.; Gao, C.; He, C.; Chen, N.; Qi, Z.; Song, L.; Jiang, J.; Zhu, J.; Xiong, Y. Isolation of Cu atoms in Pd lattice: forming highly selective sites for photocatalytic conversion of CO_2 to CH_4. *J. Am. Chem. Soc.* **2017**, *139*, 4486−4492.
(23) Bai, S.; Shao, Q.; Wang, P.; Dai, Q.; Wang, X.; Huang, X. Highly active and selective hydrogenation of CO_2 to ethanol by ordered Pd−Cu nanoparticles. *J. Am. Chem. Soc.* **2017**, *139*, 6827−6830.
(24) Zhai, H.; Alexandrova, A. N. Fluxionality of catalytic clusters: When it matters and how to address it. *ACS Catal.* **2017**, *7*, 1905−1911.
(25) Zandkarimi, B.; Alexandrova, A. N. Surface-supported cluster catalysis: Ensembles of metastable states run the show. *Wiley Interdiscip. Rev.: Comput. Mol. Sci.* **2019**, *9*, e1420.
(26) Sun, G.; Sautet, P. Metastable structures in cluster catalysis from first-principles: Structural ensemble in reaction conditions and metastability triggered reactivity. *J. Am. Chem. Soc.* **2018**, *140*, 2812−2820.
(27) Zhai, H.; Alexandrova, A. N. Local fluxionality of surface-deposited cluster catalysts: The case of Pt_7 on Al_2O_3. *J. Phys. Chem. Lett.* **2018**, *9*, 1696−1702.
(28) Zhang, Z.; Zandkarimi, B.; Alexandrova, A. N. Ensembles of metastable states govern heterogeneous catalysis on dynamic interfaces. *Acc. Chem. Res.* **2020**, *53*, 447−458.
(29) Baxter, E. T.; Ha, M.-A.; Cass, A. C.; Alexandrova, A. N.; Anderson, S. L. Ethylene dehydrogenation on Pt4, 7, 8 clusters on Al_2O_3: Strong cluster size dependence linked to preferred catalyst morphologies. *ACS Catal.* **2017**, *7*, 3322−3335.
(30) Ha, M. A.; Baxter, E. T.; Cass, A. C.; Anderson, S. L.; Alexandrova, A. N. Boron switch for selectivity of catalytic dehydrogenation on size-selected Pt clusters on Al_2O_3. *J. Am. Chem. Soc.* **2017**, *139*, 11568−11575.
(31) Li, X.; Grubisic, A.; Stokes, S. T.; Cordes, J.; Gantefoer, G. F.; Bowen, K. H.; Kiran, B.; Willis, M.; Jena, P.; Burgert, R.; Schnoeckel, H. Unexpected stability of Al_4H_6: a borane analog? *Science* **2007**, *315*, 356−358.
(32) Zhang, X.; Liu, G.; Gantefoer, G.; Bowen, K. H.; Alexandrova, A. N. $PtZnH_5^-$, A σ-aromatic cluster. *J. Phys. Chem. Lett.* **2014**, *5*, 1596−1601.
(33) Liu, G.; Ciborowski, S.; Bowen, K. Photoelectron spectroscopic and computational study of pyridine-ligated gold cluster anions. *J. Phys. Chem. A* **2017**, *121*, 5817−5822.
(34) Liu, G.; Zhu, Z.; Ciborowski, S. M.; Ariyarathna, I. R.; Miliordos, E.; Bowen, K. H. Selective Activation of the C−H Bond in Methane by Single Platinum Atomic Anions. *Angew. Chem., Int. Ed.* **2019**, *58*, 7773−7777.
(35) Buendia, F.; Beltran, M. R.; Zhang, X.; Liu, G.; Buytendyk, A.; Bowen, K. H. Ab initio and anion photoelectron study of Au_nRh_m (n = 1−7, m = 1−2) clusters. *Phys. Chem. Chem. Phys.* **2015**, *17*, 28219−28227.
(36) Liu, G.; Ciborowski, S. M.; Zhu, Z.; Bowen, K. H. Activation of hydroxylamine by single gold atomic anions. *Int. J. Mass Spectrom.* **2019**, *435*, 114−117.
(37) Lang, S. M.; Bernhardt, T. M.; Chernyy, V.; Bakker, J. M.; Barnett, R. N.; Landman, U. Selective C−H bond cleavage in methane by small gold clusters. *Angew. Chem., Int. Ed.* **2017**, *56*, 13406−13410.
(38) Jewell, L. L.; Davis, B. H. Review of absorption and adsorption in the hydrogen−palladium system. *Appl. Catal., A* **2006**, *310*, 1−15.
(39) Gerhards, M.; Thomas, O. C.; Nilles, J. M.; Zheng, W.-J.; Bowen, K. H. Cobalt−benzene cluster anions: Mass spectrometry and negative ion photoelectron spectroscopy. *J. Chem. Phys.* **2002**, *116*, 10247.
(40) Zhang, X.; Wang, Y.; Wang, H.; Lim, A.; Ganteför, G.; Bowen, K. H.; Reveles, J. U.; Khanna, S. N. On the existence of designer magnetic superatoms. *J. Am. Chem. Soc.* **2013**, *135*, 4856−4861.
(41) Robinson, P. J.; Gantefor, G.; Alexandrova, A.; Bowen, K. H. Photoelectron spectroscopic and theoretical study of the [HPd (η2-H_2)]− cluster anion. *J. Chem. Phys.* **2015**, *143*, 094307.
(42) Wang, H.; Zhang, X.; Ko, Y. J.; Gantefor, G.; Bowen, K. H.; Li, X.; Kiran, B.; Kandalam, A. K. Photoelectron spectroscopy of boron aluminum hydride cluster anions. *J. Chem. Phys.* **2014**, *140*, 164317.
(43) Graham, J. D.; Buytendyk, A. M.; Zhang, X.; Collins, E. L.; Kiran, B.; Gantefoer, G.; Eichhorn, B. W.; Gutsev, G. L.; Behera, S.; Jena, P.; Bowen, K. H. Alanate Anion, AlH_4^-: Photoelectron Spectrum and Computations. *J. Phys. Chem. A* **2014**, *118*, 8158−8162.
(44) Perdew, J. P.; Burke, K.; Ernzerhof, M. Generalized gradient approximation made simple. *Phys. Rev. Lett.* **1996**, *77*, 3865−3868.
(45) Gaussian 16, Revision C.01. Frisch, M. J.; Trucks, G. W.; Schlegel, H. B.; Scuseria, G. E.; Robb, M. A.; Cheeseman, J. R.; Scalmani, G.; Barone, V.; Petersson, G. A.; Nakatsuji, H.; Li, X.; Caricato, M.; Marenich, A. V.; Bloino, J.; Janesko, B. G.; Gomperts, R.; Mennucci, B.; Hratchian, H. P.; Ortiz, J. V.; Izmaylov, A. F.; Sonnenberg, J. L.; Williams-Young, D.; Ding, F.; Lipparini, F.; Egidi, F.; Goings, J.; Peng, B.; Petrone, A.; Henderson, T.; Ranasinghe, D.; Zakrzewski, V. G.; Gao, J.; Rega, N.; Zheng, G.; Liang, W.; Hada, M.; Ehara, M.; Toyota, K.; Fukuda, R.; Hasegawa, J.; Ishida, M.; Nakajima, T.; Honda, Y.; Kitao, O.; Nakai, H.; Vreven, T.; Throssell, K.; Montgomery, J. A., Jr.; Peralta, J. E.; Ogliaro, F.; Bearpark, M. J.; Heyd, J. J.; Brothers, E. N.; Kudin, K. N.; Staroverov, V. N.; Keith, T. A.; Kobayashi, R.; Normand, J.; Raghavachari, K.; Rendell, A. P.; Burant, J. C.; Iyengar, S. S.; Tomasi, J.; Cossi, M.; Millam, J. M.; Klene, M.; Adamo, C.; Cammi, R.; Ochterski, J. W.; Martin, R. L.; Morokuma, K.; Farkas, O.; Foresman, J. B.; Fox, D. J. Gaussian, Inc., Wallingford CT, 2016.
(46) Hay, P. J.; Wadt, W. R. Ab initio effective core potentials for molecular calculations. Potentials for the transition metal atoms Sc to Hg. *J. Chem. Phys.* **1985**, *82*, 270−283.
(47) Wadt, W. R.; Hay, P. J. Ab initio effective core potentials for molecular calculations. Potentials for main group elements Na to Bi. *J. Chem. Phys.* **1985**, *82*, 284−298.
(48) Hay, P. J.; Wadt, W. R. Ab initio effective core potentials for molecular calculations. Potentials for K to Au including the outermost core orbitals. *J. Chem. Phys.* **1985**, *82*, 299−310.
(49) Peterson, K. A.; Puzzarini, C. Systematically convergent basis sets for transition metals. II. Pseudopotential-based correlation consistent basis sets for the group 11 (Cu, Ag, Au) and 12 (Zn, Cd, Hg) elements. *Theor. Chem. Acc.* **2005**, *114*, 283−296.
(50) Čížek, J. On the use of the cluster expansion and the technique of diagrams in calculations of correlation effects in atoms and molecules. *Adv. Chem. Phys.* **2007**, *14*, 35−89.
(51) Purvis, G. D.; Bartlett, R. J. A full coupled-cluster singles and doubles model: The inclusion of disconnected triples. *J. Chem. Phys.* **1982**, *76*, 1910−1918.
(52) Scuseria, G. E.; Janssen, C. L.; Schaefer, H. F. An efficient reformulation of the closed-shell coupled cluster single and double excitation (CCSD) equations. *J. Chem. Phys.* **1988**, *89*, 7382−7387.
(53) Scuseria, G. E.; Schaefer, H. F. Is coupled cluster singles and doubles (CCSD) more computationally intensive than quadratic configuration interaction (QCISD)? *J. Chem. Phys.* **1989**, *90*, 3700−3703.
(54) Hegarty, D.; Robb, M. A. Application of unitary group methods to configuration interaction calculations. *Mol. Phys.* **1979**, *38*, 1795−1812.

https://dx.doi.org/10.1021/jacs.0c01855
J. Am. Chem. Soc. 2020, 142, 7930−7936

(55) Eade, R. H. A.; Robb, M. A. Direct minimization in mc scf theory. The quasi-newton method. *Chem. Phys. Lett.* **1981**, *83*, 362−368.
(56) Schlegel, H. B.; Robb, M. A. MC SCF gradient optimization of the $H_2CO \rightarrow H_2 + CO$ transition structure. *Chem. Phys. Lett.* **1982**, *93*, 43−46.
(57) Bernardi, F.; Bottoni, A.; McDouall, J. J. W.; Robb, M. A.; Schlegel, H. B. MCSCF gradient calculation of transition structures in organic reactions. *Faraday Symp. Chem. Soc.* **1984**, *19*, 137.
(58) Frisch, M.; Ragazos, I. N.; Robb, M. A.; Bernhard Schlegel, H. An evaluation of three direct MC-SCF procedures. *Chem. Phys. Lett.* **1992**, *189*, 524−528.
(59) Yamamoto, N.; Vreven, T.; Robb, M. A.; Frisch, M. J.; Bernhard Schlegel, H. A direct derivative MC-SCF procedure. *Chem. Phys. Lett.* **1996**, *250*, 373−378.
(60) Siegbahn, P. E. M. A new direct CI method for large CI expansions in a small orbital space. *Chem. Phys. Lett.* **1984**, *109*, 417−423.
(61) Robb, M. A.; Niazi, U. *The Unitary Group Approach to Electronic Structure Computations*; CRC Press: Boca Raton, FL, 1990.
(62) Klene, M.; Robb, M. A.; Frisch, M. J.; Celani, P. Parallel implementation of the CI-vector evaluation in full CI/CAS-SCF. *J. Chem. Phys.* **2000**, *113*, 5653−5665.
(63) Reed, A. E.; Weinstock, R. B.; Weinhold, F. Natural population analysis. *J. Chem. Phys.* **1985**, *83*, 735−746.

https://dx.doi.org/10.1021/jacs.0c01855
J. Am. Chem. Soc. 2020, 142, 7930−7936